The Astrophysical Journal, 624:223–231, 2005 May 1

ULTRAVIOLET RADIATION INSIDE INTERSTELLAR GRAIN AGGREGATES. I. THE DENSITY OF RADIATION

Cesare Cecchi-Pestellini
Osservatorio Astronomico di Cagliari, Loc. Poggio dei Pini, Strada 54, 09012 Capoterra, Italy

Rosalba Saija, Maria Antonia Iatì, Arianna Giusto, Ferdinando Borghese, and Paolo Denti
Dipartimento di Fisica della Materia e Tecnologie Fisiche Avanzate, Università di Messina, Salita Sperone 31, 98166 Messina, Italy; iati@ortica.unime.it

and

Santi Aiello
Dipartimento di Astronomia e Scienza dello Spazio, Università di Firenze, Largo Enrico Fermi 5, 50125 Florence, Italy
Received 2004 December 20; accepted 2005 January 20

ABSTRACT

We study the distribution of energy density inside dust grain aggregates through an approach based on the multipole expansion of the electromagnetic fields. A significant fraction of the energy of the impinging wave is found throughout the interiors of grains. Implications for extraterrestrial prebiotic chemistry are discussed.

Subject headings: astrobiology — dust, extinction — radiative transfer

1. INTRODUCTION

Recent laboratory experiments demonstrate the synthesis of amino acids, basic ingredients in all vital processes, when ice mixtures representative of cold interstellar grain mantles were subjected to ultraviolet (UV) irradiation (Bernstein et al. 2002; Muñoz Caro et al. 2002). Fifty years before, Miller (1953) reported the remarkable results he had achieved by the action of electric discharge on a mixture of the reducing gases CH_4, NH_3, H_2O, and H_2 that simulated what was viewed at the time as possible primitive Earth conditions. Although the chemical compositions of the target mixtures appear very similar (e.g., Gibb et al. 2004), reaction pathways leading to the formation of complex organics are profoundly different, because under interstellar conditions low temperatures preclude most chemical reactions that are efficient in the Miller apparatus.

However, in the complex process leading to the formation of circumstellar disks around young stars from prestellar dense molecular clouds, physical conditions similar to those of terrestrial laboratories might be present. In a gas containing dust grains, aggregation occurs naturally as the result of ballistic collisions, producing loosely packed structures with much of their internal volume being vacuum (cavities). It is this internal volume that leads to a completely different chemical scenario with respect to that on the surface of grains (Duley 2000). In the interior of dust aggregates UV radiation, X-rays, cosmic rays, thermal shocks, etc., induce a secondary chemistry in which the reaction products cannot escape the cavity. This gives rise to a peculiar situation, as the chemistry is offered high-temperature, high-density, and reducing conditions in a transient gas phase with rapid quenching of the reaction products.

The effective production of complex molecules depends critically on the dose of UV radiation impinging on the molecular material trapped in a grain (Cecchi-Pestellini et al. 2005). Within the complex interplay of the molecular formation and destruction processes, the radiation field carries out a dual role. If, on the one hand, it might be one of the most important destruction mechanisms, on the other hand, it drives the production of new molecular species, with the creation of reactive ions and radicals in the mixture. Since even a small amount of UV radiation has profound chemical consequences on the molecular content of the cavity, a knowledge of the radiation density distribution inside an interstellar aggregate is essential in order to understand the plausibility and efficiency of the proposed mechanism. To derive the UV radiation density distribution inside the aggregate cavity, we use a technique based on the multipole expansion of the electromagnetic field, already tested in treating the scattering of light by arbitrarily shaped, porous, composite particles (Borghese et al. 2002). Grain aggregates are assumed to be fluffily substructured collections of dust particles covered by ice mantles, loosely attached to one another. Each particle consists of a single material, such as silicates or carbon, as formed in the various separate sources of cosmic dust. Voids are naturally generated by random accretion of particles leading to cavities of sizes comparable to those of the coagulating grains. Basic constituents of the aggregate might also be porous. Two kinds of cavities are then considered: (1) interstitial cavities that form because of the aggregation process and (2) central cavities aimed at simulating porous aggregating particles.

In § 2 we present an outline of the modeling approach exploited in calculating the electromagnetic field inside a sphere composed of several concentric layers. We also describe the technique for calculating the scattered field just outside the surface of the spheres composing an aggregate. Numerical simulations of the energy density of UV radiation expected inside an aggregate are presented in § 3. Calculations are performed for both central and interstitial cavities. Section 4 contains our conclusions.

2. THE MODEL

In order to calculate the electromagnetic field inside the interiors of and at the surfaces of the clustered spheres, we use a method developed to compute the optical properties of morphologically complex particles (Saija et al. 2001; Borghese et al. 2002; Iatì et al. 2004). Although the present technique resorts to the multipole expansion of the electromagnetic field, it does not imply any far-field approximation. We describe first how to calculate the field inside a radially nonhomogeneous

sphere excited by a plane wave field. Then we consider the field in the near zone of an aggregate of radially nonhomogeneous spheres, in particular at their surfaces. In both cases we assume that all the fields depend on time through the factor $\exp(-i\omega t)$, which is omitted throughout, and define the propagation constant in vacuo $k_v = \omega/c$. The surrounding medium is homogenous, nonabsorbing, and isotropic, with refractive index n and propagation constant $k = nk_v$. The incident field is the plane wave

$$\boldsymbol{E}_I = E_0 \hat{\boldsymbol{e}} \exp(i\boldsymbol{k}_I \cdot \boldsymbol{r}), \tag{1}$$

where $\hat{\boldsymbol{e}}$ is the unit polarization vector and $\boldsymbol{k}_I = k\hat{\boldsymbol{k}}_I$ is the propagation vector.

2.1. *Single Nonhomogenous Sphere*

In this section we consider a radially nonhomogeneous sphere with radius ρ and complex refractive index $n_0 = n_0(r)$. In the region external to the sphere the field is the superposition of $\boldsymbol{E}_I$, equation (1), and the scattered field $\boldsymbol{E}_S$. Both fields are expanded in a series of spherical vector multipole fields. We define the vector multipole fields $\boldsymbol{H}$ as (Rose 1957)

$$\begin{aligned} \boldsymbol{H}^{(1)}_{lm}(\boldsymbol{r}, K) &= h_l(Kr)\boldsymbol{X}_{lm}(\hat{\boldsymbol{r}}), \\ \boldsymbol{H}^{(2)}_{lm}(\boldsymbol{r}, K) &= \frac{1}{K}\nabla \times \boldsymbol{H}^{(1)}_{lm}(\boldsymbol{r}, K), \end{aligned} \tag{2}$$

where $\boldsymbol{X}_{lm}$ are vector spherical harmonics (Jackson 1975), h_l are spherical Hankel functions of the first kind, and the superscripts (1) and (2) refer to the values of parity index p appropriate to the magnetic and electric multipoles, respectively. The $\boldsymbol{H}$ multipole fields satisfy the radiation condition at infinity. We also define the multipole fields $\boldsymbol{J}$, which are regular at the origin: they are identical to the $\boldsymbol{H}$ fields, except for the substitution of the spherical Bessel functions j_l in place of the Hankel functions h_l. We expand the electric fields outside the sphere as

$$\boldsymbol{E}_{\rm ext} = \boldsymbol{E}_S + \boldsymbol{E}_I = E_0 \sum_{plm} \left[A^{(p)}_{lm} \boldsymbol{H}^{(p)}_{lm}(\boldsymbol{r}, k) + W^{(p)}_{lm} \boldsymbol{J}^{(p)}_{lm}(\boldsymbol{r}, k) \right], \tag{3}$$

where the amplitudes of the incident field $W^{(p)}_{lm}$ are defined by Borghese et al. (2002) and the amplitudes $A^{(p)}_{lm}$ are determined by the boundary conditions at the surface of the scattering sphere. Since it does not imply any far-field approximation, expansion (3) is valid everywhere outside the sphere.

Both the internal electric and magnetic fields satisfy, not the customary Helmholtz equation, but rather the equations

$$\begin{aligned} \nabla \times \nabla \times \boldsymbol{E} - n_0^2(r) k_v^2 \boldsymbol{E} &= 0, \\ \nabla \times \nabla \times \boldsymbol{B} - n_0^2(r) k_v^2 \boldsymbol{B} &= -ik_v \nabla n_0^2(r) \times \boldsymbol{E}, \end{aligned} \tag{4}$$

which are coupled because of the assumed nonhomogeneity of the material. Nevertheless, the internal field can still be expanded in a series of vector spherical harmonics in the form (Wyatt 1962; Borghese et al. 1987)

$$\boldsymbol{E}_T = \sum_{lm} \left[C^{(1)}_{lm} \Phi_l(r) \boldsymbol{X}_{lm}(\hat{\boldsymbol{r}}) + C^{(2)}_{lm} \frac{1}{n_0^2} \frac{1}{k_v} \nabla \times \Psi_l(r) \boldsymbol{X}_{lm}(\hat{\boldsymbol{r}}) \right], \tag{5}$$

$$i\boldsymbol{B}_T = \sum_{lm} \left[C^{(1)}_{lm} \frac{1}{k_v} \nabla \times \Phi_l(r) \boldsymbol{X}_{lm}(\hat{\boldsymbol{r}}) + C^{(2)}_{lm} \Psi_l(r) \boldsymbol{X}_{lm}(\hat{\boldsymbol{r}}) \right], \tag{6}$$

which, for any choice of the radial functions and for any radial dependence of the refractive index, satisfies the Maxwell equations $\nabla \cdot \boldsymbol{B} = 0$ and $\nabla \cdot n_0^2 \boldsymbol{E} = 0$. The equations

$$\begin{aligned} \left[\frac{d^2}{dr^2} - \frac{l(l+1)}{r^2} + k_v^2 n_0^2 - \frac{2}{n_0} \frac{dn_0}{dr} \frac{d}{dr} \right] r\Psi_l(r) = 0, \\ \left[\frac{d^2}{dr^2} - \frac{l(l+1)}{r^2} + k_v^2 n_0^2 \right] r\Phi_l(r) = 0 \end{aligned} \tag{7}$$

are derived by substituting equations (5) and (6) into equation (4). The solutions to these equations are the radial functions $\Psi_l(r)$ and $\Phi_l(r)$, which are regular at the origin. The equations (7) are integrated numerically. When $n_0(r)$ reduces to a constant, equations (4) are identical to each other and to the Helmholtz equation, which in turn means that equations (7) are identical to each other. In this case the normalization can be chosen so that $\Phi_l = \Psi_l = j_l(n_0 k_v r)$.

By imposing the customary boundary conditions across the surface of the sphere, the mutual independence of the vector spherical harmonics yields, for each l and m, four equations among which the amplitudes of the internal field $C^{(p)}_{lm}$ can be easily eliminated. We then get the amplitudes of the scattered field in the form

$$A^{(p)}_{lm} = -R^{(p)}_l W^{(p)}_{lm}, \tag{8}$$

with

$$R^{(p)}_l = \frac{G^{(p)\prime}_l(x) u_l(x) - (1 + \bar{n}\delta_{p2})^2 G^{(p)}_l(x) u'_l(x)}{G^{(p)\prime}_l(x) w_l(x) - (1 + \bar{n}\delta_{p2})^2 G^{(p)}_l(x) w'_l(x)}, \tag{9}$$

where $x = k\rho$, $\bar{n} = [n_0(\rho)/n] - 1$, and

$$G^{(1)}_l(kr) = kr\Phi_l(r), \quad G^{(2)}_l(kr) = kr\Psi_l(r). \tag{10}$$

Once the amplitudes $A^{(p)}_{lm}$ have been calculated, the amplitudes $C^{(p)}_{lm}$ are derived and thus the field at any point inside the sphere.

The above theory can be applied to layered spheres, e.g., to the case of the spheres composed of two concentric homogenous layers of refractive indexes n_- and n_+ considered in § 3. In order to save the continuity of both the refractive index and its radial derivative across the two materials, a thin transition layer is placed at the interface. In this layer, defined by the radial interval $r_- \le r \le r_+$, the refractive index varies from n_- to n_+ according to the rule

$$n_0^2(r) = n_-^2 + (3s^2 - 2s^3)\Delta, \tag{11}$$

where we define the quantities

$$\Delta = n_+^2 - n_-^2, \quad s = \frac{r - r_-}{r_+ - r_-}. \tag{12}$$

Provided the transition layer is thin enough, the scattering properties of the sphere are not altered within numerical accuracy (Borghese et al. 1987). From numerical integration of the radial equations and knowledge of the amplitudes $C^{(p)}_{lm}$ we are then able to calculate the internal field at any point inside the sphere.

2.2. *Cluster of Spheres*

The optical response of a grain aggregate can be obtained starting from those of single constituent spheres. The cluster is composed of a number $\mathcal{N}$ of basic spherical units, labeled by the

index α, of radius ρ_α and refractive index n_α. The centers of the spheres are located at $\boldsymbol{R}_\alpha$. The field scattered by the whole aggregate is the superposition of the fields scattered by each sphere,

$$\boldsymbol{E}_S = \sum_\alpha \sum_{plm} \boldsymbol{H}_{lm}^{(p)}(\boldsymbol{r}_\alpha, k)\mathcal{A}_{\alpha lm}^{(p)}, \tag{13}$$

where $\boldsymbol{r}_\alpha = \boldsymbol{r} - \boldsymbol{R}_\alpha$. If the spherical units are homogeneous, the field inside the αth sphere is expanded as

$$\boldsymbol{E}_{T\alpha} = \sum_{plm} \boldsymbol{J}_{lm}^{(p)}(\boldsymbol{r}_\alpha, k_\alpha)\mathcal{C}_{\alpha lm}^{(p)}, \tag{14}$$

with $k_\alpha = n_\alpha k_v$, so that it is regular everywhere inside the sphere. If the spheres are radially nonhomogeneous, the expansion of the internal field is instead given by equation (5). The magnetic field, necessary for imposing the boundary conditions, is given by the equation

$$i\boldsymbol{B} = \frac{1}{k_v} \nabla \times \boldsymbol{E} \tag{15}$$

both inside and outside the spheres. The scattered field is given by a linear combination of multipole fields that have different origins, whereas the incident field is given by a combination of multipole fields centered at the origin of the coordinates. Since the boundary conditions must be imposed at the surface of each constituent sphere, we resort to the addition theorem for multipole fields (Borghese et al. 1980) to define $\boldsymbol{E}_S$ (eq. [13]) in terms of multipole fields centered at $\boldsymbol{R}_\alpha$. The scattered field at the surface of the αth sphere becomes

$$\boldsymbol{E}_S = \sum_{plm} \left[\boldsymbol{H}_{lm}^{(p)}(\boldsymbol{r}_\alpha, k)\mathcal{A}_{\alpha lm}^{(p)} + \sum_{\alpha'} \sum_{p'l'm'} \boldsymbol{J}_{lm}^{(p)}(\boldsymbol{r}_\alpha, k)\mathcal{H}_{\alpha lm\alpha' l'm'}^{(pp')}\mathcal{A}_{\alpha' l'm'}^{(p')} \right], \tag{16}$$

where the quantities $\mathcal{H}$ are given in Borghese et al. (1980, 2002). Analogously, the incident field at the surface of the αth sphere is

$$\boldsymbol{E}_I = \sum_{plm} \sum_{p'l'm'} \boldsymbol{J}_{lm}^{(p)}(\boldsymbol{r}_\alpha, k)\mathcal{J}_{\alpha lm0l'm'}^{(p,p')} W_{1l'm'}^{(p')}, \tag{17}$$

where the quantities $\mathcal{J}$ are once again defined in Borghese et al. (1980, 2002). We impose the boundary conditions by the same technique exploited for homogeneous spheres. Accordingly, we get for each α, l, and m four equations among which the eliminations of the amplitudes of the internal field are trivial. The final result is a system of linear nonhomogeneous equations

$$\sum_{\alpha'} \sum_{p'l'm'} \mathcal{M}_{\alpha lm\alpha' l'm'}^{(pp')}\mathcal{A}_{\alpha' l'm'}^{(p')} = -\mathcal{W}_{I\alpha lm}^{(p)}, \tag{18}$$

where we define

$$\mathcal{W}_{I\alpha lm}^{(p)} = \sum_{p'l'm'} \mathcal{J}_{\alpha lm0l'm'}^{(pp')} W_{Il'm'}^{(p')}, \tag{19}$$

$$\mathcal{M}_{\alpha lm\alpha' l'm'}^{(pp')} = \left(R_{\alpha l}^{(p)}\right)^{-1} \delta_{\alpha\alpha'}\delta_{pp'}\delta_{ll'}\delta_{mm'} + \mathcal{H}_{\alpha lm\alpha' l'm'}^{(pp')}. \tag{20}$$

When the spheres are homogeneous, the quantities $R_{\alpha l}^{(p)}$ coincide with the Mie coefficients for the αth sphere; for radially nonhomogeneous spheres, these quantities are given by equation (9). The matrix $\mathbf{H}$, of elements $\mathcal{H}_{\alpha lm\alpha' l'm'}^{(pp')}$, describes the multiple scattering processes.

The formal solution to the system reported above can be written as

$$\mathcal{A}_{\alpha lm}^{(p)} = -\sum_{p'l'm'} \left[\mathbf{M}^{-1}\right]_{\alpha lm\alpha' l'm'}^{(pp')} \mathcal{W}_{I\alpha' l'm'}^{(p')}, \tag{21}$$

where the matrix $\mathbf{M}^{-1}$ relates the amplitudes of the incident field to those of the fields scattered by each sphere in the aggregate. Once the amplitudes $\mathcal{A}_{\alpha lm}^{(p)}$ are derived, it is straightforward to calculate the field at the surface of any sphere of the cluster and the amplitudes $\mathcal{C}_{\alpha lm}^{(p)}$, which are related to the fields inside the spheres composing the aggregate.

3. THE FIELD INSIDE THE AGGREGATE CAVITIES

In this section we present results of the calculations of the UV radiation dose inside both the central and the interstitial cavities. We first derive the time-averaged distribution of the electromagnetic energy density

$$w(\boldsymbol{r}) = \frac{\epsilon|\boldsymbol{E}_T|^2 + (1/\mu)|\boldsymbol{B}_T|^2}{16\pi} \tag{22}$$

inside homogeneous spheres made of astronomical silicates (Suh 1999) and amorphous carbon (Suh 2000), with and without a central cavity. Both materials have $\mu = 1$ but a complex dielectric function ϵ, so the energy density is complex. The imaginary part when multiplied by 2ω gives the rate of dissipation (Ishimaru 1978). In the whole set of related contour plots (see Figs. 1–3), we show the logarithm of both the real and imaginary parts of the energy density in the interior of spheres with a radius $r_0 = 50$ nm. In the figures the energy density is reported in a gray scale, increasing from black to white in steps of 0.5. Figure 1 displays results for homogeneous spheres of astronomical silicates and amorphous carbon in a plane through the centers of the spheres. We report only the case of polarization orthogonal to the plane of the plot because the distribution of the energy density in a plane, e.g., parallel to the polarization vector differs little. Contour plots for spheres of the same radius but containing centered voids of different sizes are shown in Figure 2 for grains made of carbonaceous materials and in Figure 3 for silicate particles. The incident wave has $\lambda = 0.1$ μm and unit amplitude, i.e., unit energy density. Carbonaceous materials present large changes in the energy density distribution because of the large imaginary part of their refractive index. The presence of intense dissipation spots inside the interstitial material suggests the possibility of a highly nonuniform distribution of temperature in spite of their smallness. Anisotropic radiation energy deposition combined with dishomogeneities in the chemical composition of interstitial materials might favor excess infrared emission from large interstellar carbon grains, as originally suggested by Duley & Williams (1988).

In Figure 4 we show the logarithm of the distribution of the real part of the energy density on the internal surface of the cavities as a function of the polar angle θ measured from the direction of the incident wavevector. In Figure 5 we report the logarithm of the real part of the energy density as a function of $q = z/r_0$ along a line through the centers of the spheres parallel to the incident wavevector (aligned with the z-axis). As in the contour plots (Figs. 2 and 3), there is an evident difference in the behavior of silicates and carbonaceous materials. However, in both materials the internal fields have strength comparable to that of the incident

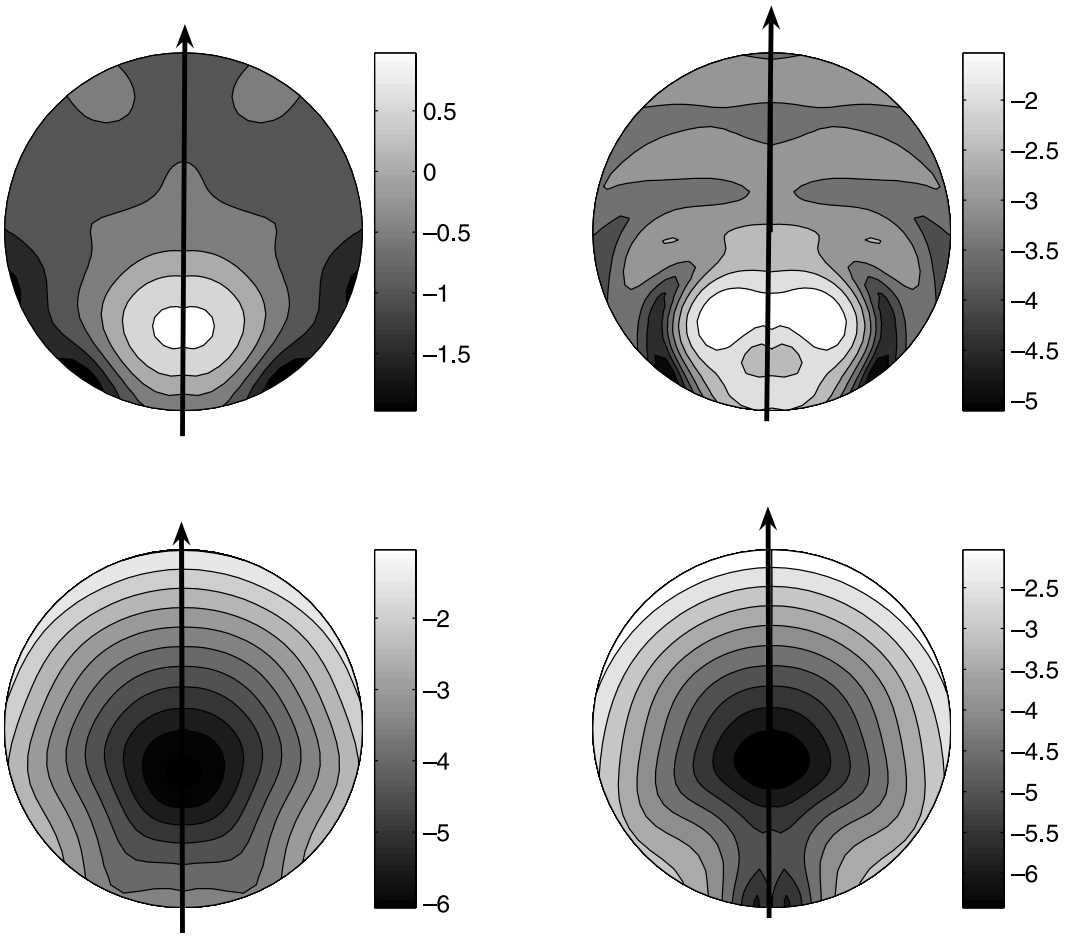

FIG. 1.—Contour plots of the logarithm of the real (*left*) and imaginary parts (*right*) of the energy density inside homogeneous spheres of amorphous carbon (*top*) and astronomical silicates (*bottom*). The radius of the spheres is $r_0 = 50$ nm, and the wavelength of the incident wave is $\lambda = 0.1$ μm. The polarization of the incident field is orthogonal to the plane of the figure.

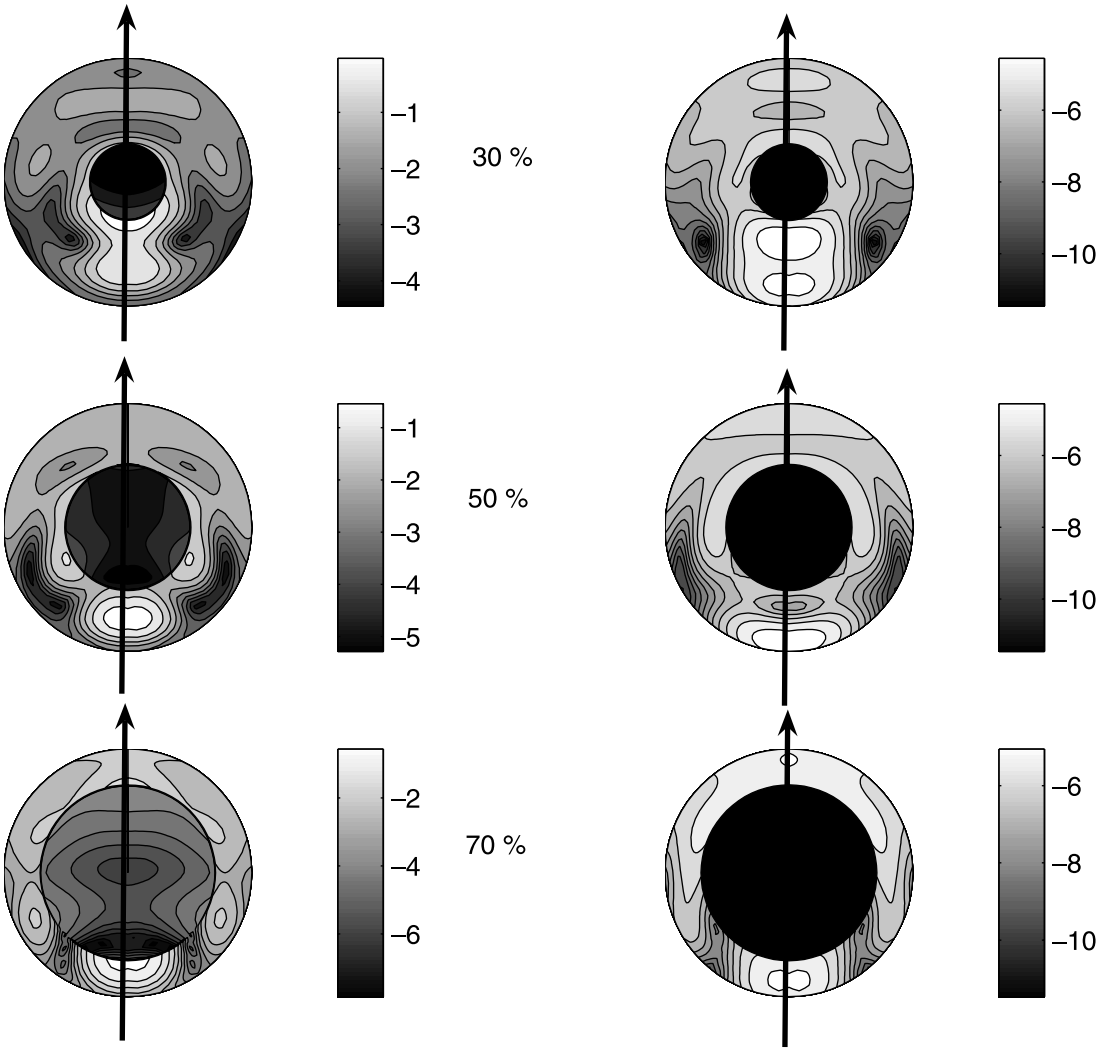

FIG. 2.—Contour plots of the logarithm of the real (*left*) and imaginary parts (*right*) of the energy density inside amorphous carbon spheres containing central spherical voids of different radii. The radius of the spheres is $r_0 = 50$ nm. The radius of the internal cavity is reported for each pair of panels as a percentage of the radius of the host sphere. The wavelength of the incident wave is $\lambda = 0.1$ μm, and the polarization of the incident field is orthogonal to the plane of the figure.

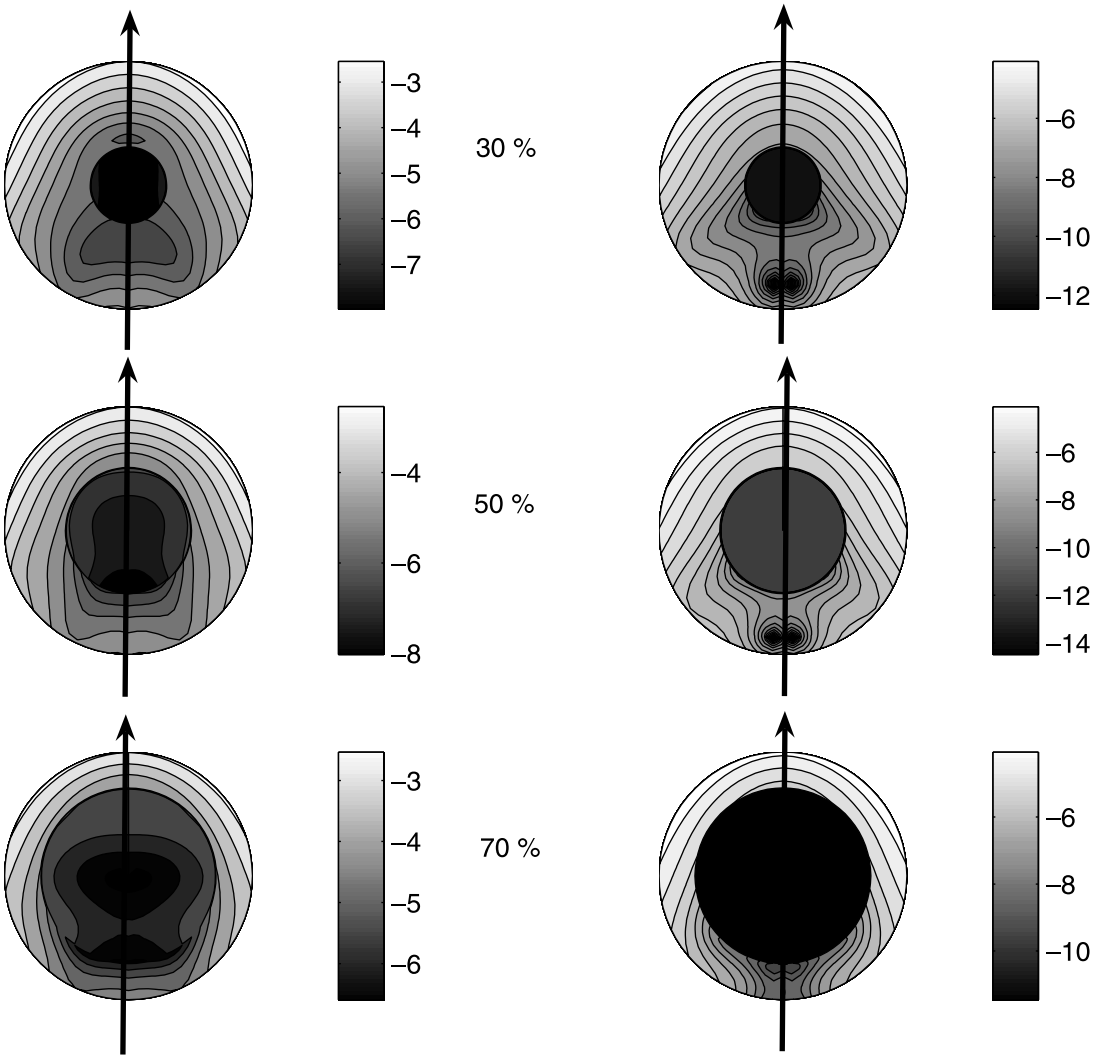

FIG. 3.—Same as in Fig. 2, but for silicate grains.

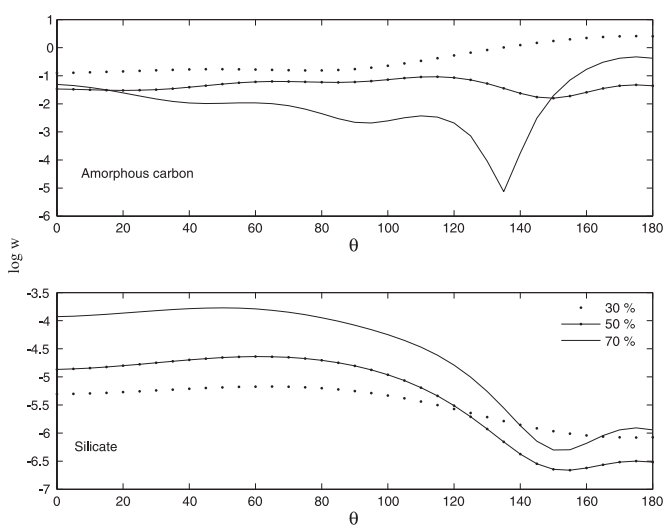

FIG. 4.—Plot of the logarithm of the real part of the energy density for the same grains of Figs. 2 and 3 on the internal surface of the cavity, in a plane orthogonal to the polarization vector, as a function of the polar angle θ measured from the direction of the incident wavevector.

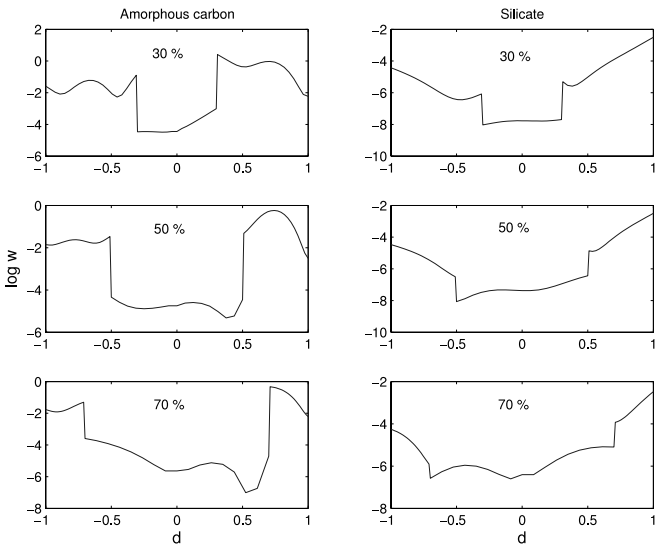

FIG. 5.—Plot of the logarithm of the real part of the energy density for the same grains of Figs. 2 and 3 along the z-axis (taken parallel to the incident wavevector) as a function of $d = z/r_0$.

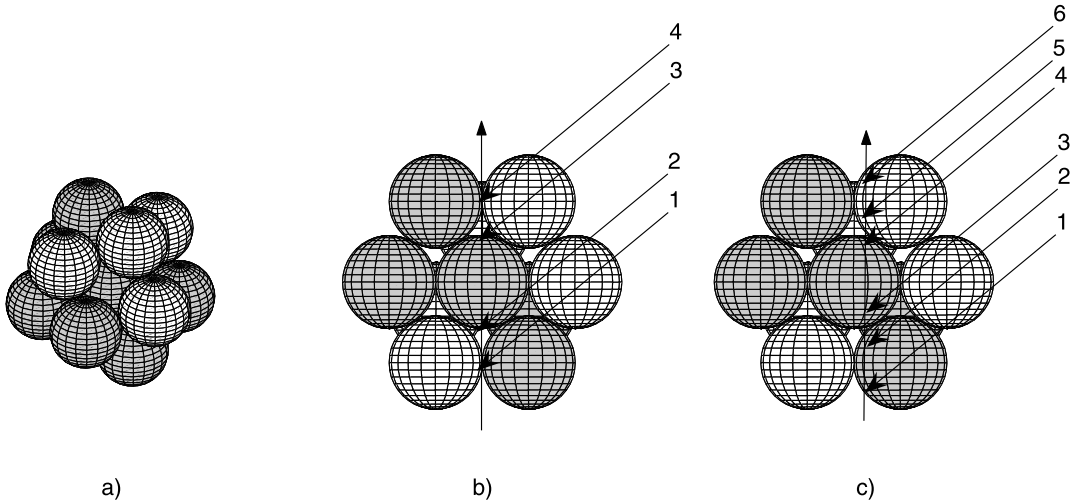

FIG. 6.—(*a*) Adopted shape of the aggregate reference model. (*b*) Line parallel to the incident wavevector crossing the *x*-*y* plane at $x = 0$, $y = 0$ intercepts four points over the aggregate surface. (*c*) Line parallel to the incident wavevector crossing the *x*-*y* plane at $x = 0$, $y = 30$ nm intercepts six points over the aggregate surface. Darker spheres in (*b*) and (*c*) represent silicate units, and lighter ones represent carbon units.

wave, in spite of the high imaginary part of the refractive index. Figures 4 and 5 also show that, in at least one case, there is a spot in which the energy density is larger than that of the incident field. This is not surprising, as what really matters for the correctness of the results is that the Poynting theorem, which requires volume integration, is satisfied.

We now consider a plane wave impinging on a grain aggregate. We adopt as a reference model a grain aggregate composed of $\mathcal{N} = 13$ spherical subunits clustered in the roughly spherical shape shown in Figure 6*a*. Grains have similar volume fractions of silicates and carbonaceous materials, $f_{\rm sil} = 7/6 f_{\rm C}$. Therefore, we assume that seven spheres have the refractive index of silicates and the remaining six have that of the carbonaceous material. This choice gives the grain as a whole optical properties akin to those of silicates mixed with carbonaceous materials (e.g., GEMS; Bradley et al. 1999). The radius of the spherical basic constituents of the aggregate is chosen to be $r_m = 20$ nm, consistent with a recent evaluation of the IR and visible extinction and polarization of composite interstellar grains (Wurm & Schnaiter 2002). The diameter of aggregates results in $D_g = 120$ nm. The coordinates of the centers of the aggregate units (in nanometers) are reported in Table 1.

TABLE 1
COORDINATES OF THE CENTERS OF THE SPHERES

Number	*x*	*y*	*z*
1*.....	0.0000000	0.0000000	0.0000000
2*.....	0.0000000	40.000000	0.0000000
3*.....	0.0000000	20.000000	34.641016
4*.....	0.0000000	−20.000000	−34.641016
5*.....	32.659863	−20.000000	−11.547005
6*.....	−32.659863	20.000000	−11.547005
7*.....	−32.659863	−20.000000	−11.547005
8.....	0.0000000	−40.000000	0.0000000
9.....	0.0000000	−20.000000	34.641016
10.....	0.0000000	20.000000	−34.641016
11.....	32.659863	20.000000	−11.547005
12.....	−32.659863	0.0000000	23.094011
13.....	32.659863	0.0000000	23.094011

NOTES.—All values are given in nanometers. The rows marked with an asterisk refer to spheres of silicates; the other spheres are of carbonaceous material.

Monomers are not homogeneous because coagulation is likely to occur when dust grains have already accreted an ice mantle. Therefore, we assume that the single spherical units are covered with a layer of condensed gas (mainly water), whose width is taken as $\Delta r = 5$ nm, which corresponds roughly to 20 monolayers. Thus, the ice volume filling factor results in $f_{\rm ice} \sim 0.5$. Dielectric constants of water ice are given by Warren (1984). Physicochemical properties of the aggregate reference model are summarized in Table 2.

The (unit) incident wave is linearly polarized normally to the plane of the figure (e.g., Figs. 6*b*–6*c*). The energy density is computed just outside the surface of the spheres at the points of intersection of two lines parallel to the incident wavevector. As shown in Figures 6*b* and 6*c*, these lines cross the surface of the clustered spheres at four and six points, respectively. The energy density, which in this case is real, cannot be represented as in the single-sphere calculations (e.g., Figs. 1–3). Therefore, we resort to bar diagrams with each bar proportional to the energy density at a particular point of intersection. The intersection points are labeled as in Figures 6*b*–6*c*. Note that points 1 and 4 in Figure 6*b* are the points of contact between a carbonaceous and a silicate sphere. Results are presented in Figures 7 and 8 for some representative wavelengths. The density of radiation is larger at shorter wavelengths and tends to decrease with increasing wavelength. The field scattered by a nonspherical particle has a rather complicated space dependence in the near zone. Our results show that the largest values of the energy density occur at points that are on the internal surface of interstitial cavities.

TABLE 2
PHYSICOCHEMICAL PROPERTIES OF THE AGGREGATE REFERENCE MODEL

Parameter	Value
Number of units, $\mathcal{N}$	13
Aggregate size, D_g (nm)	120
Monomer size, $2r_m$ (nm)	40
Mantle width, Δr (nm)	5
Ice fraction, $f_{\rm ice}$	∼0.5
Silicate to carbon ratio, $f_{\rm sil}/f_{\rm C}$	7:6

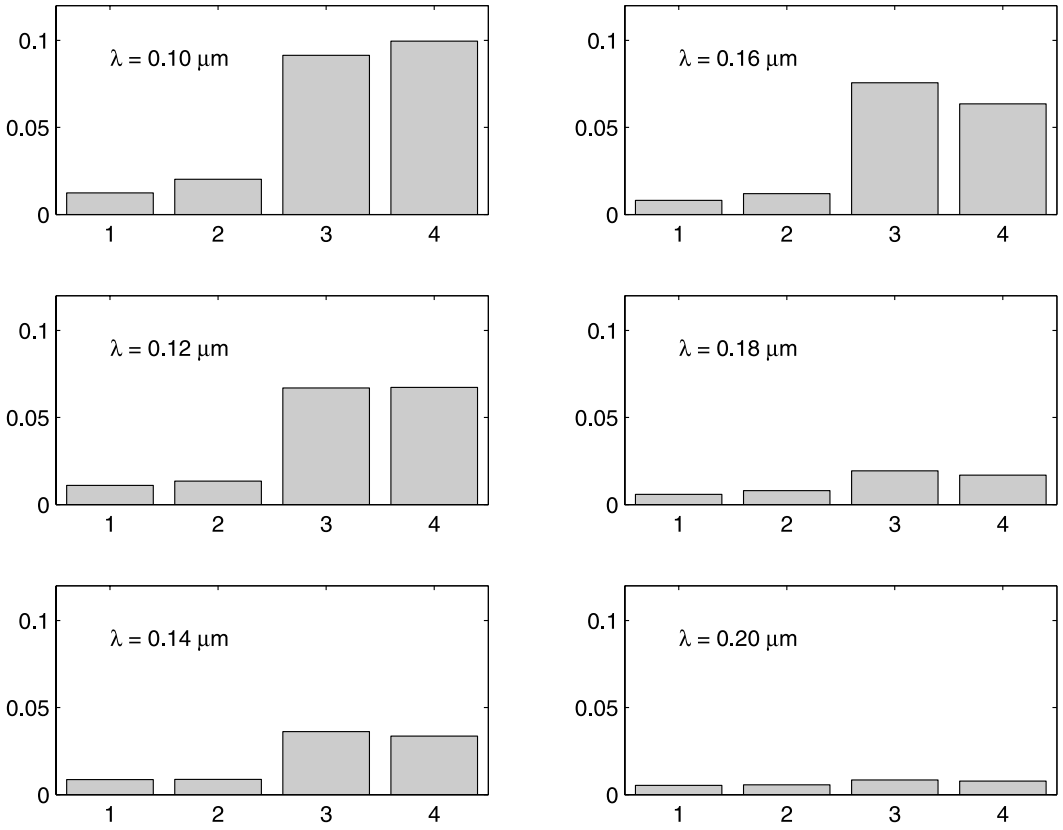

FIG. 7.—Energy densities at the four intersection points depicted in Fig. 6*b*. The wavelengths of the incident radiation are reported in each panel.

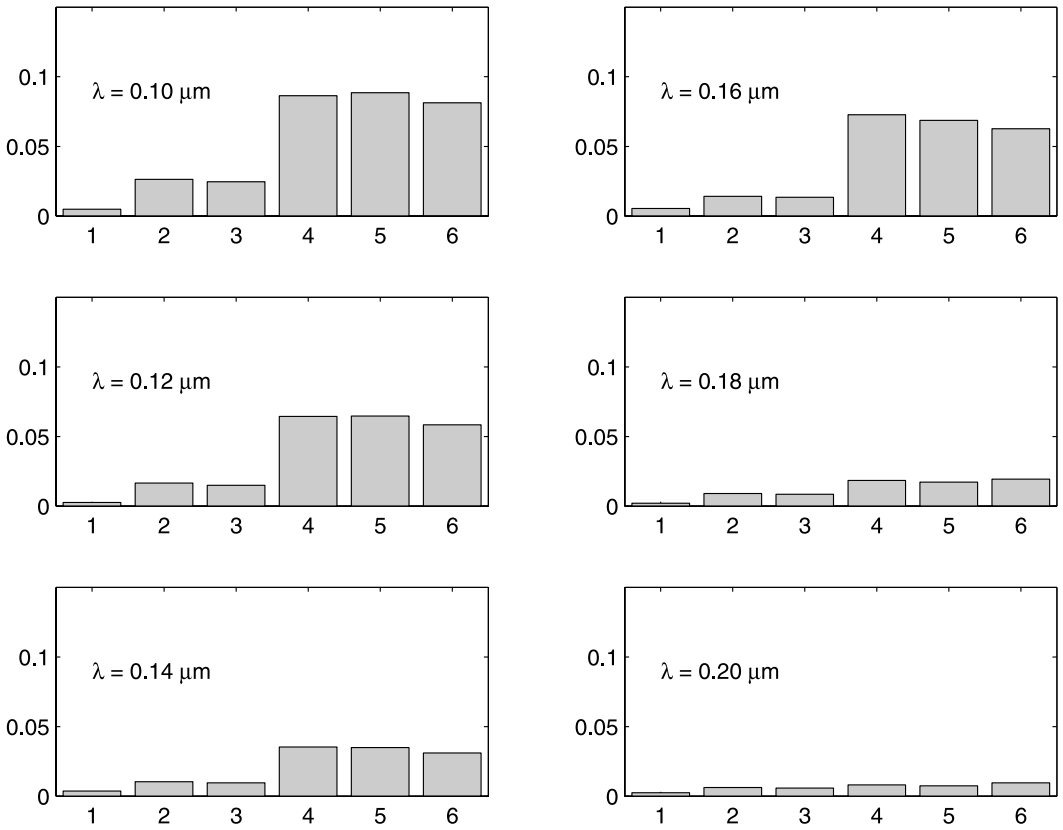

FIG. 8.—Energy densities at the six intersection points depicted in Fig. 6*c*. The wavelengths of the incident radiation are reported in each panel.

All these results imply that if the aggregates are embedded in a strong radiation field, their interiors are also well illuminated.

4. CONCLUSIONS

In this work, we have presented a detailed treatment of the penetration of UV radiation inside an interstellar grain. The research was stimulated by the works of Duley (2000) and Cecchi-Pestellini et al. (2005), who noted that the chemistry inside porous or aggregate grains presents a completely different scenario with respect to that on the surface of grains or in the gas phase. The existence of an efficient biochemistry proceeding in the interior of dust grains during the early stages of the solar system formation has implications for the origin of life. Indeed, dust grains not only might contain the right environment in which the organic matter formed and survived in space, but also might be the vehicles able to seed planetary systems with the prebiotic molecules needed for the synthesis of proteins and nucleic acids in living organisms.

This work constitutes the foundation for an investigation, which we will present elsewhere, aimed at characterizing possible prebiotic chemical pathways under exposure conditions similar to those relevant within the primordial nebula. The results presented in § 3 show that porous and aggregate grains are efficiently illuminated throughout their interiors. The energy density in the cavities is a significant fraction of the one carried by the incident wave. Thus, if an aggregate grain is exposed to large radiation fields for enough time, the inner ice mixture may become enriched with a significant number of radicals. After a collision or a cosmic-ray impact, radicals and molecules from the ice enter a transient, warm, high-pressure gas phase (Cecchi-Pestellini et al. 2005).

Instead of the search for new mechanisms of production of biomolecules, the focus of this study is on the special *habitat* provided by the interior of interstellar grains, where well-known tested working processes, i.e., radical chemistry in reducing conditions, might proceed efficiently. In this picture, cavities inside grain aggregates filled with interstellar ices become microreactors where stellar high-energy photons and particles can ignite chemical reactions in planetary-like physical conditions. The reaction products stored inside grain aggregates would also be partly shielded from the extremely unfavorable environmental conditions of the early stages of Sun life (Feigelson & Montmerle 1999). The Miller experiment appears thus revisited through innumerable repetitions inside dust grains.

The study of meteorites, particularly the carbonaceous chondrites that contain a significant fraction of organic matter, has allowed close examination of extraterrestrial organic material delivered to the Earth. The enriched deuterium content points to an interstellar genesis from the deuterium-enriched presolar nebula (Epstein et al. 1987). In the Murchison meteorite more than 70 amino acids have been found, eight of them occurring in proteins (Cronin et al. 1988). Moreover, a variety of sugars, in amounts comparable to those of amino acids, was discovered in the Murchison and Murray meteorites (Cooper et al. 2001). Biomolecules are in general chiral and almost exclusively homochiral. Of the 20 protein amino acids, 19 are chiral and of the L-conformation. Sugars are also chiral, but they are of the D-conformation. Cronin & Pizzarello (1997) found 9% L-enantiomeric excess for nonbiological amino acids, which cannot be suspected to be the result of biological contamination. These findings seem to push the problem of the origin of biological chirality out into the cosmos.

Among the many scenarios put forward to explain the origin of this chiral homogeneity (i.e., homochirality), one involves the asymmetric photolysis of amino acids present in space, triggered by circularly polarized ultraviolet radiation (Bailey 2001 and references therein). In the second paper of this series, we will argue that inside the cavities of porous grains, linearly polarized UV radiation depolarizes, i.e., becomes elliptically polarized. As a consequence, cavities inside dust grains might provide a suitable environment in which interstellar molecules can evolve and be selected into complex prebiotic species.

REFERENCES

Bailey, J. 2001, Origins Life Evol. Biosphere, 31, 167
Bernstein, M. P., Dworkin, J. P., Sandford, S. A., Cooper, G. W., & Allamandola, L. J. 2002, Nature, 416, 401
Borghese, F., Denti, P., & Saija, R. 2002, Scattering from Model Nonspherical Particles (London: Springer)
Borghese, F., Denti, P., Saija, R., Toscano, G., & Sindoni, O. I. 1987, J. Opt. Soc. Am. A, 4, 1984
Borghese, F., Denti, P., Toscano, G., & Sindoni, O. I. 1980, J. Math. Phys., 21, 2754
Bradley, J. P., et al. 1999, Science, 285, 1716
Cecchi-Pestellini, C., Scappini, F., Saija, R., Iatì, M. A., Giusto, A., Aiello, S., Borghese, F., & Denti, P. 2005, Int. J. Astrobiology, in press
Cooper, G., Kimmich, N., Belisle, W., Sarinana, J., Brabham, K., & Garrel, L. 2001, Nature, 414, 879
Cronin, J. R., & Pizzarello, S. 1997, Science, 275, 951
Cronin, J. R., Pizzarello, S., & Cruikshank, D. P. 1988, in Meteorites and the Early Solar System, ed. J. F. Kerridge & M. S. Matthews (Tucson: Univ. Arizona Press), 819
Duley, W. W. 2000, MNRAS, 319, 791
Duley, W. W., & Williams, D. A. 1988, MNRAS, 231, 969
Epstein, S., Krishnamurthy, R. V., Cronin, J. R., Pizzarello, S., & Yuen, G. U. 1987, Nature, 326, 477
Feigelson, E. D., & Montmerle, T. 1999, ARA&A, 37, 363
Gibb, E. L., Whittet, D. C. B., Boogert, A. C. A., & Tielens, A. G. G. M. 2004, ApJS, 151, 35
Iatì, M. A., Giusto, A., Saija, R., Borghese, F., Denti, P., Cecchi-Pestellini, C., & Aiello, S. 2004, ApJ, 615, 286
Ishimaru, A. 1978, Wave Propagation and Scattering in Random Media (New York: Academic)
Jackson, J. D. 1975, Classical Electrodynamics (New York: Wiley)
Miller, S. L. 1953, Science, 117, 528
Muñoz Caro, G. M., et al. 2002, Nature, 416, 403
Rose, E. M. 1957, Elementary Theory of Angular Momentum (New York: Wiley)
Saija, R., Iatì, M. A., Borghese, F., Denti, P., Aiello, S., & Cecchi-Pestellini, C. 2001, ApJ, 559, 993
Suh, K.-W. 1999, MNRAS, 304, 389
———. 2000, MNRAS, 315, 740
Warren, S. G. 1984, Appl. Opt., 23, 1206
Wurm, G., & Schnaiter, M. 2002, ApJ, 567, 370
Wyatt, P. J. 1962, Phys. Rev. B, 127, 1771

The Astrophysical Journal, 632:1204–1206, 2005 October 20

ERRATUM: "ULTRAVIOLET RADIATION INSIDE INTERSTELLAR GRAIN AGGREGATES. I. THE DENSITY OF RADIATION" (ApJ, 624, 223 [2005])

Cesare Cecchi-Pestellini
Osservatorio Astronomico di Cagliari, Capoterra, Italy

Rosalba Saija, Maria Antonia Iatì, Arianna Giusto, Ferdinando Borghese, and Paolo Denti
Dipartimento di Fisica della Materia e Tecnologie Fisiche Avanzate, Università di Messina, Italy

and

Santi Aiello
Dipartimento di Astronomia e Scienza dello Spazio, Università di Firenze, Italy

Figures 1, 2, 4, and 5 of the original paper are incorrect, and might frustrate any attempt to reproduce our results. These figures were obtained using an incorrect value of the refractive index for the amorphous carbon grains, different from the one quoted (K.-W. Suh, MNRAS, 315, 740 [2000]). Although the energy density distribution calculated with the correct refractive index is numerically different from the one reported, the conclusions of the paper are unchanged.

We thank Harald Mutschke of the Friedrich Schiller University Jena, for calling our attention to this point.

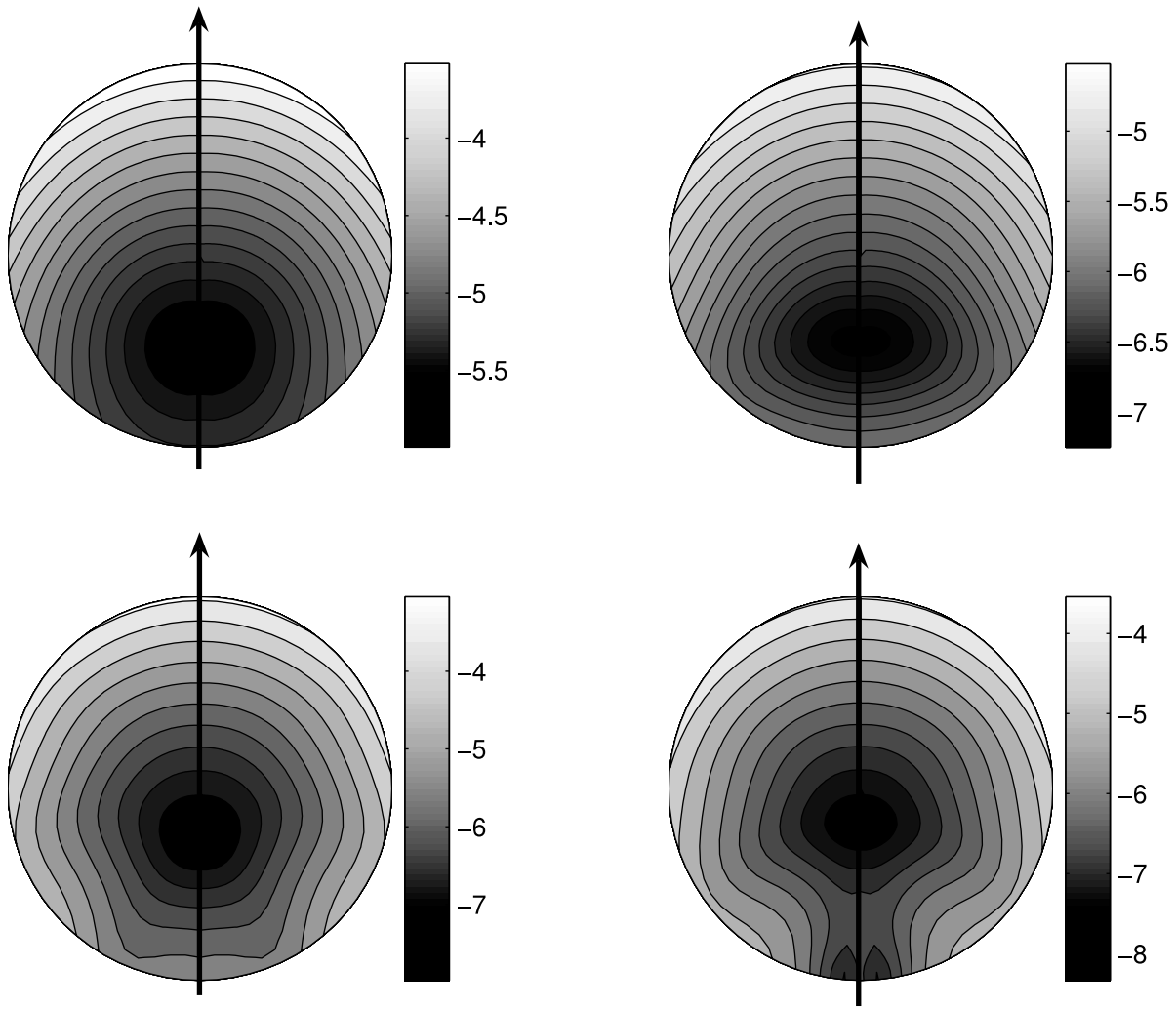

Fig. 1.—Contour plots of the logarithm of the real (*left*) and imaginary parts (*right*) of the energy density inside homogeneous spheres of amorphous carbon (*top*) and astronomical silicates (*bottom*). The radius of the spheres is $r_0 = 50$ nm, and the wavelength of the incident radiation is $\lambda = 0.1$ μm. The polarization of the incident field is orthogonal to the plane of the figure.

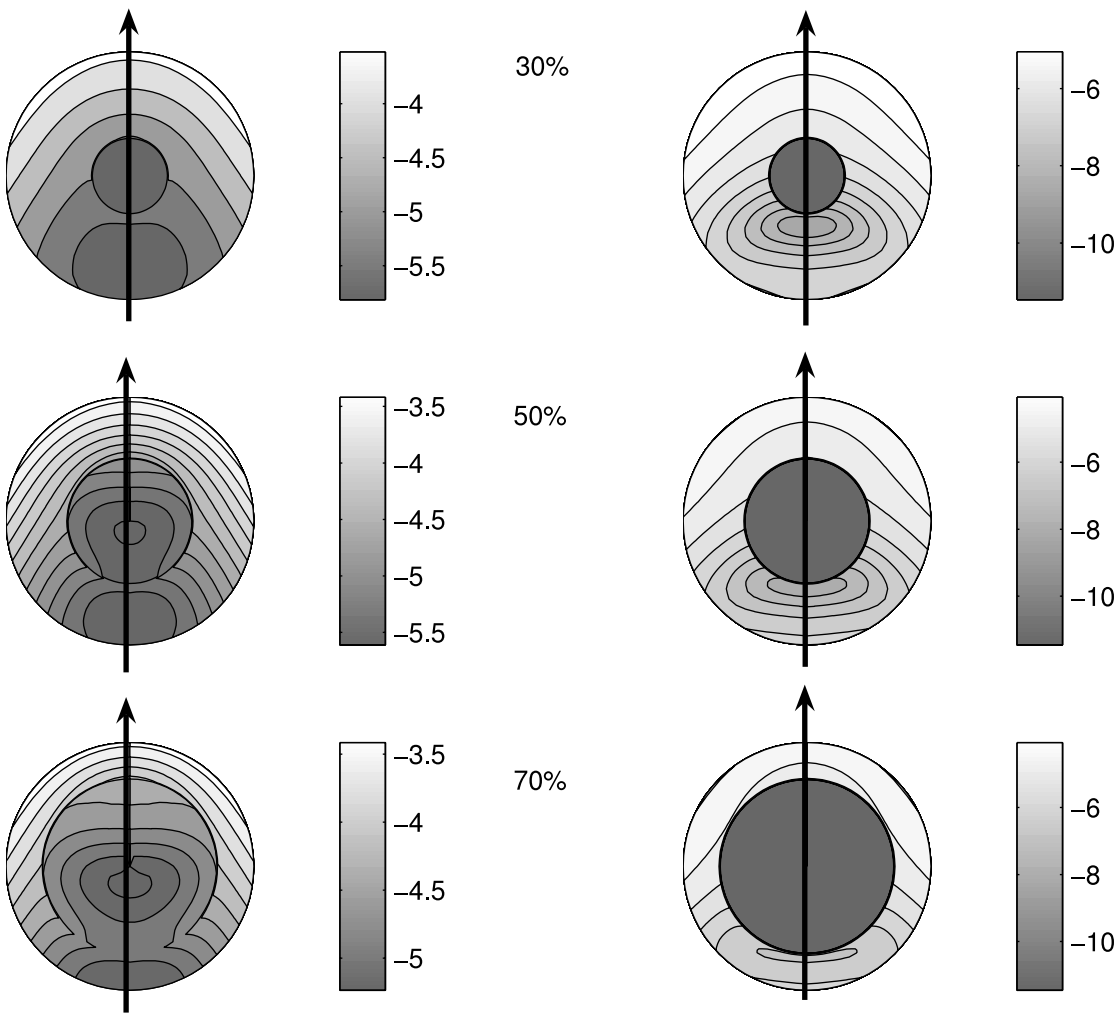

FIG. 2.—Contour plots of the logarithm of the real (*left*) and imaginary parts (*right*) of the energy density inside amorphous carbon spheres containing central spherical voids of different radii. The radius of the spheres is $r_0 = 50$ nm. The radius of the internal cavity is reported for each couple of panels as a percentage of the radius of the host sphere. The wavelength of the incident radiation is $\lambda = 0.1$ μm, and the polarization of the incident field is orthogonal to the plane of the figure.

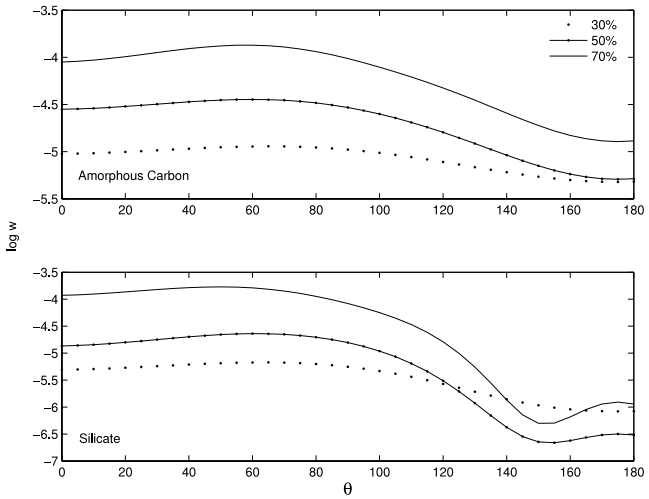

FIG. 4.—Plot of the logarithm of the real part of the energy density for the same grains of Figs. 2 and 3 on the internal surface of the cavity, in a plane orthogonal to the polarization vector, as a function of the polar angle θ measured from the direction of the incident wavevector.

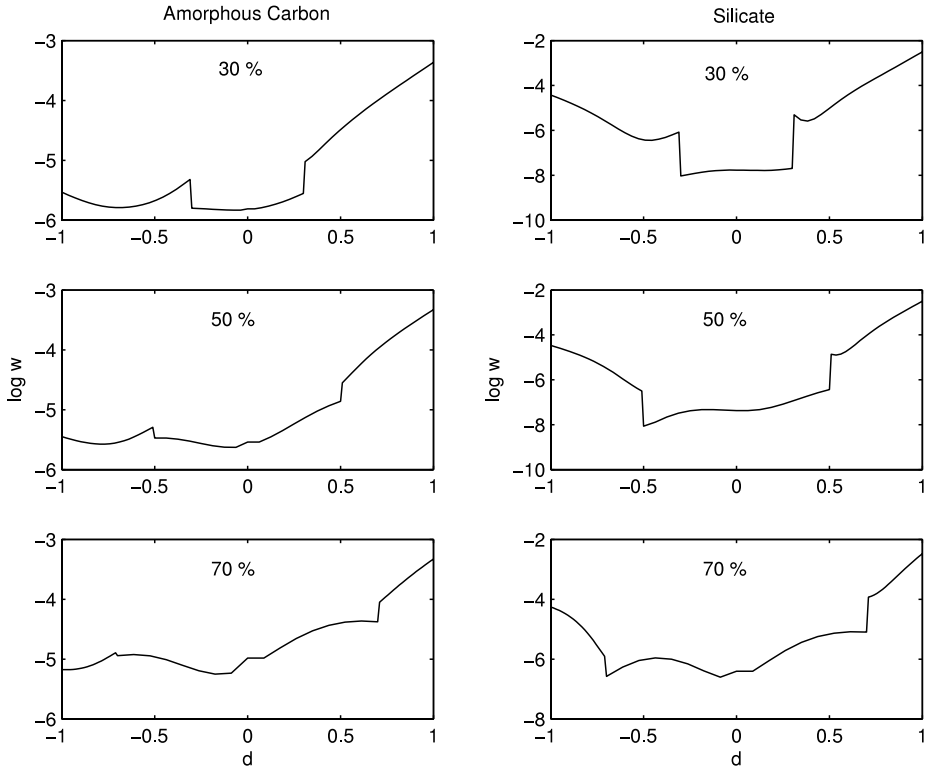

FIG. 5.—Plot of the logarithm of the real part of the energy density for the same grains of Figs. 2 and 3 along the z axis (taken parallel to the incident wavevector) as a function of $d = z/r_0$.